analytical chemistry

Article

Cite This: *Anal. Chem.* 2019, 91, 8170–8175

pubs.acs.org/ac

Light-Responsive Metal–Organic Framework as an Oxidase Mimic for Cellular Glutathione Detection

Yufeng Liu,[†] Min Zhou,[†] Wen Cao,[†] Xiaoyu Wang,[†] Quan Wang,[†] Sirong Li,[†] and Hui Wei*[,†,‡]

[†]Department of Biomedical Engineering, College of Engineering and Applied Sciences, Nanjing National Laboratory of Microstructures, Jiangsu Key Laboratory of Artificial Functional Materials, Nanjing University, Nanjing, Jiangsu 210093, China

[‡]State Key Laboratory of Analytical Chemistry for Life Science and State Key Laboratory of Coordination Chemistry, School of Chemistry and Chemical Engineering, Collaborative Innovation Center of Chemistry for Life Sciences, Nanjing University, Nanjing, Jiangsu 210023, China

Supporting Information

ABSTRACT: Nanomaterials with enzyme-like characteristics (nanozymes) have been developed to mimic enzymes because of their low cost, high stability, and large-scale production. By using light as an external stimulation, one can modulate nanozymes' catalytic activities with controlled spatial and temporal precision. A few inorganic photoactive materials have been investigated to construct light-responsive oxidase-like nanozymes. However, these materials suffered from limited absorbance of visible light. To address this challenge, herein we have developed a photosensitized metal–organic framework (PSMOF) by using a derivative of $Ru(bpy)_3^{2+}$ with stronger visible-light absorption as a PS linker. The PSMOF exhibited excellent oxidase-like activity, which could be modulated by switching light on and off. Moreover, the PSMOF was used to detect glutathione levels in both normal and cancer cells with good selectivity and high sensitivity. This study not only provides a smart strategy to modulate nanozymes' activities but also broadens the sensing applications of nanozymes.

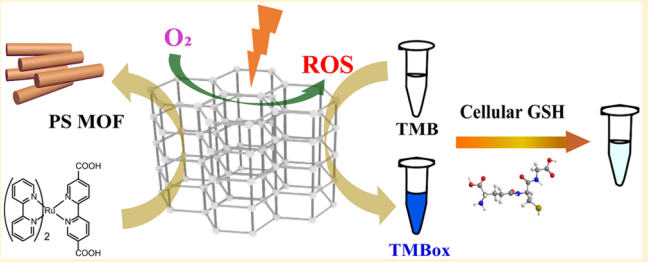

Natural enzymes are miraculous catalysts for thousands of biological reactions. Their practical applications, however, have been limited because of their low stability in nonphysiological environment, high cost for production, and difficulty in storage. To overcome these drawbacks, nanomaterials with enzyme-like characteristics (called nanozymes) have been developed to mimic various enzymes because of their advantages such as low-cost, high stability, and large-scale production.[1−18]

To further make nanozymes as better alternatives to enzymes, several strategies have been explored to modulate their catalytic activities,[19] such as controlling the size,[20,21] morphology,[22−24] and composition of the nanozymes,[25−28] forming hybrids,[29−31] using external stimuli,[32−34] and so on. Among these strategies, using light to stimulate the nanozyme catalysis is of great promise due to the efficient control with spatial and temporal precision as well as environmental friendliness. To fulfill this promise, highly efficient photoresponsive nanomaterials have been investigated for mimicking natural enzymes in recent years.[35−39] For example, Xia et al. demonstrated that the peroxidase-like activity of gold nanoparticles (AuNPs) could be enhanced by photoinduced hot electrons for the catalytic oxidation of 3,3′,5,5′-tetramethylbenzydine (TMB) with hydrogen peroxide (H_2O_2).[40]

On the other hand, by using oxidase-like nanozymes, the unstable H_2O_2 could be avoided. To this end, photoresponsive oxidase mimics can be employed to activate oxygen for oxidizing substrates under light irradiation. Until now, metal clusters,[41] metal oxides,[42] and metal halides[43] have been used to construct light-responsive oxidase-like nanozymes. Despite great success, these materials suffer from limited absorbance of visible light. We reasoned that one can tackle this challenge by using organic dyes with stronger visible-light absorption. To protect organic dyes from dimerization in aqueous solution and self-degradation under oxidation, herein we incorporated them as photoactive ligands within metal–organic frameworks (MOFs).[44] We chose MOFs because not only of their porous and crystalline nature for integrating large amounts of photosensitive organic linkers but also their efficient mass transport for catalysis and narrow pores for reducing the interference from large biomolecules in bioanalysis.[45−50]

Herein, we designed and synthesized a photosensitized MOF (PSMOF) by introducing a photoactive ligand, a $Ru(bpy)_3^{2+}$ derivative, within a Zn-based MOF. The PSMOF effectively catalyzed the oxidation of model oxidase substrates (i.e., TMB, OPD, and ABTS) under visible-light irradiation, showing excellent oxidase-like activity. By switching on/off the light, we regulated the oxidase-like activity of the PSMOF, demonstrating the as-designed light-responsive property.

Received: January 29, 2019
Accepted: May 31, 2019
Published: May 31, 2019

DOI: 10.1021/acs.analchem.9b00512
Anal. Chem. 2019, 91, 8170–8175

Moreover, the PSMOF was employed as a colorimetric probe for detection of glutathione (GSH) in cells.

EXPERIMENTAL SECTION

Reagents and Materials. Commercially available reagents were used without further purification. *cis*-[$Ru(bpy)_2Cl_2$] was purchased from Suzhou Xinjiayuan Chemical Reagent Co., Ltd. (Jiangsu, China). 2,2′-Bipyridine 5,5′-dicarboxylated acid was purchased from Shuya Medicine Technology Co., Ltd. (Shanghai, China). 4,4′-Biphenyldicarboxylic acid and mannitol were obtained from Energy Chemical Co., Ltd. (Shanghai, China). $Zn(NO_3)_2{\cdot}6H_2O$, 3,3′,5,5′-tetramethylbenzidine dihydrochloride (TMB), 2,2′-azinobis (3-ethyl benzothiazoline-6-sulfonic acid) ammonium (ABTS), L-cysteine (L-Cys), bovine serum albumin, L-histidine, L-glutamic acid, 5,5-dimethyl-1-pyridine *N*-oxide (DMPO), and glucose were purchased from Aladdin Chemical Co. Ltd. (Shanghai, China). Hydrogen peroxide (H_2O_2), DL-tryptophan, L-ascorbic acid, DL-methionine, and *o*-phenylenediamine (OPD) were purchased from Sinopharm Chemical Reagent Co. Ltd. (Shanghai, China). L-Alanine was obtained from Huixing Biochemical Co., Ltd. (Shanghai, China). Glutathione (GSH) was obtained from J&K Scientific. Human serum albumin (HSA) was obtained from CSL Behring AG (Switzerland). Catalase was obtained from Nanjing Henghuang Biotechnology (Jiangsu, China). Superoxide dismutase was obtained from Sigma-Aldrich. The GSH assay kit was obtained from Solarbio Life Science Co., Ltd. (Beijing, China). All aqueous solutions were prepared with deionized water (18.2 MΩ·cm, Millipore).

Synthesis of PS Organic Linker and the PSMOF. The PS linker was synthesized by following a previous procedure with minor revisions.[51] *cis*-[$Ru(bpy)_2Cl_2$] (320 mg, 0.66 mmol) and 2,2′-bipyridine 5,5′-dicarboxylated acid (202 mg, 0.84 mmol) were mixed in 50 mL of EtOH/H_2O (1:1), refluxed at 90 °C for 12 h under N_2 protection, and then concentrated. The solid was recrystallized from a MeOH/diethyl ether mixture. As shown in Figure S1, ^1H NMR (DMSO-d_6, 400 MHz): δ 8.89−8.99 (m, 6H), 8.38 (d, 2H), 8.10−8.21 (m, 4H), 7.98 (s, 2H), 7.78 (d, 4H), 7.55 (t, 2H), 7.49 (t, 2H).

Mixture of the PS organic linker (4.7 mg) and 4,4′-biphenyldicarboxylic acid (52 mg) was reacted with $Zn(NO_3)_2{\cdot}6H_2O$ (33 mg) in *N*,*N*′-dimethylformamide (DMF) (4 mL) under solvothermal conditions (100 °C, 12 h). After filtration, red-yellow crystals with feather-like shapes were obtained and redispersed in DMF.

Visible-Light-Responsive Oxidase Mimic of the PSMOF. In general, 10 μL of the PSMOF (3 mg/mL) and 10 μL of TMB (25 mM) were injected into 480 μL of 0.10 M HAc/NaAc buffer solution (pH 4.0). The substrate solution was irradiated using the 300 W Xe lamp with a filter above 400 nm for 2 min to activate the dissolved oxygen for oxidizing TMB. Subsequently, the UV−vis absorption spectra were collected.

Effect of Different Scavengers on the Catalytic Activity of the PSMOF. Different scavengers were respectively added into every sample solution. The buffer was 0.1 M HAc/NaAc (pH 4.0). The final concentrations of substrates is as follows: PSMOF (20 μg/mL), TMB (500 μM), mannitol (5 mM), tryptophan (2.5 mg/mL), catalase (200 U/mL), superoxide dismutase (300 U/mL), and ethanol (10% vt). The mixed solution was then under 300 W Xe lamp (with a filter above 400 nm) illumination for different times.

Spin Trapping−ESR tests. The PSMOF (20 μL, 3 mg/mL) was mixed with DMPO (100 mM) in 0.1 M HAc/NaAc (pH 4.0) solution. After being illuminated for 5 min, the mixture was characterized by a Bruker EMX-10/12 spectrometer operating at the X-band frequency (9.7 GHz) at room temperature.

Detection of GSH by the PSMOF. Typically, for colorimetric detection, 10 μL of the PSMOF (3 mg/mL), 10 μL of TMB (25 mM), and different concentration of GSH were added into 0.1 M HAc/NaAc buffer solution (pH 4.0). The final volume of the mixed solution was adjusted to 0.5 mL with the buffer. The solution was irradiated using a 300 W Xe lamp with a filter above 400 nm for 2 min and was then used for UV−vis measurements.

Cell Culture and Lysate Preparation. Cells were cultured in high-glucose Dulbecco's modified Eagle's medium (DMEM) supplemented with 10% FBS and 1% penicillin−streptomycin (10 000 U/mL) under an atmosphere of 5% CO_2 at 37 °C. When the cell density reached 80%, the HeLa (1.25×10^6) and LO2 (1.25×10^6) cells were collected and washed with chilled phosphate-buffered saline (PBS) three times, and then, the cell precipitations were suspended in 500 μL of chilled lysis buffer [0.15 M NaCl, 5 mM EDTA, 1% Triton-X 100, 10 mM Tris-HCl (pH 7.4) with appropriate protease inhibitor]. These cells were disrupted by ultrasonication for 1 min under low power, and all processes were operated at low temperature. Then, the cell lysate was centrifuged at 4 °C for 20 min at 13 000 rpm. The supernatants were transferred to sterile tubes for the following detection assays: Typically, 10 μL of PSMOF (3 mg/mL), 10 μL of TMB (25 mM) and different amounts of HeLa and LO2 lysate were added into 0.1 M HAc/NaAc buffer solution (pH 4.0). The final volume of the mixed solution was adjusted to 0.5 mL with the buffer and then the solution was irradiation using 300 W Xe lamp with a filter above 400 nm for 2 min. After centrifugation at 10 000 rpm for 2 min, the absorbance of TMB_{ox} at 652 nm was collected on a Microplate reader.

Instrumentation. ^1H NMR spectra were recorded on a Bruker AM400 spectrometer with tetramethylsilane (TMS) as an internal standard. UV−vis absorption spectra were collected on a UV−vis spectrophotometer with a 1 cm quartz cell (Beijing Purkinje General Instrument Co. Ltd., China). Transmission electron microscopy (TEM) was performed on a Tecnai F20 transmission electron microscope (FEI) at an acceleration voltage of 200 kV. Powder X-ray diffraction (PXRD) data were collected on an ARL SCINTAC X'TRA diffractometer using Cu Kα radiation (Thermo). Scanning electron microscopy (SEM) imaging was performed on a Hitachi S-4800 scanning electron microscope operating at 5 kV. A 300 W Xe lamp with a filter above 400 nm was used for light irradiation (CEL-HXF300/CEL-HXUV300, Zhongjiaojingyuan, Beijing, China). A microplate reader (SpectraMax M2e, Molecular Devices Co., Ltd., Sunnyvill, USA) recorded the absorbance of TMB_{ox} at 652 nm for the detection of cellular GSH.

RESULTS AND DISCUSSION

Synthesis and Characterization of the PSMOF. As shown in Scheme S1, [bis(2,2′-bipyridine,N_1,$N_{1'}$)(5,5′-dicarboxy-2,2′-bipydine)-ruthenium(II)] dichloride as the PS linker was synthesized by reacting *cis*-[$Ru(bpy)_2Cl_2$] with 2,2′-bipyridine-5,5′-dicarboxylate acid. NMR and UV−vis spectroscopic measurements confirmed the successful synthesis

DOI: 10.1021/acs.analchem.9b00512
Anal. Chem. 2019, 91, 8170−8175

(Figures S1 and S2). To obtain the PSMOF, the as-synthesized PS linker was mixed with 4,4′-biphenyldicarboxylic acid (H_2BPDC) and zinc nitrate hexahydrate in DMF at 100 °C for 12 h (Scheme 1). The formation of the PSMOF was first

Scheme 1. Synthesis of the PSMOF

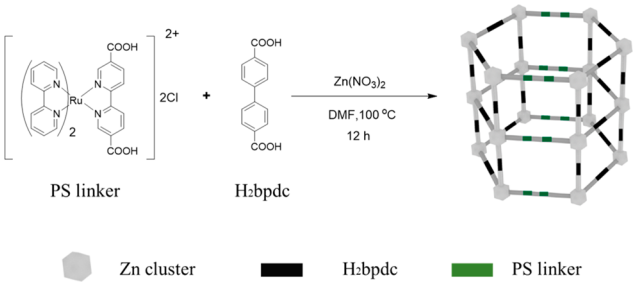

studied by transmission electron microscopy (TEM) and scanning electron microscopy (SEM). As shown in Figures 1A,B, S3, and S4, the PSMOF with a rod shape was obtained.

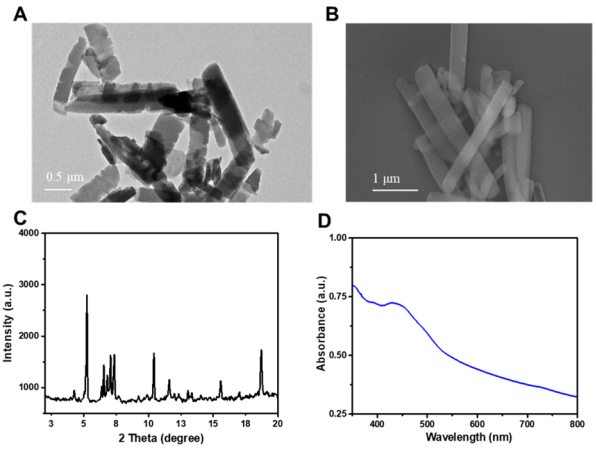

Figure 1. (A) TEM image of the PSMOF. (B) SEM image of the PSMOF. (C) PXRD pattern of the PSMOF. (D) UV−vis absorption spectrum of the PSMOF.

The powder X-ray diffraction (PXRD) pattern of the PSMOF in Figure 1C revealed that the PSMOF crystallized in the orthorhombic $C222_1$ space group, and the framework was built from linking $[Zn_2(\mu_2\text{-}CO_2)_3]$ secondary building units (SBUs) with ditopic BPDC and PS linkers.[51] UV−vis spectroscopy was measured to confirm the incorporation of the PS linker within the PSMOF. As shown in Figure 1D, the PSMOF showed strong and broad adsorption in the range of 350−800 nm, the characteristic adsorption assigned to metal-to-ligand charge transfer (MLCT) of the $Ru(bpy)_3^{2+}$ derivative,[52] indicating the successful incorporation of the PS linker within the PSMOF.

Light-Responsive Oxidase-Mimicking Activity of the PSMOF. To evaluate the visible-light-induced oxidase-mimicking activity of the PSMOF, UV−vis spectroscopy was used to monitor the catalytic oxidation of a typical oxidase chromogenic substrate TMB in 0.10 M acetate buffer (pH 4.0). As shown in Figure 2A, under the light irradiation, the PSMOF catalyzed the oxidation of TMB and produced a deep blue color. The oxidized TMB (TMB_{ox}) showed a strong UV−vis absorption peak at 652 nm, demonstrating the oxidase-like activity of the PSMOF. In contrast, without the light irradiation, TMB mixed with PSMOF produced neither a

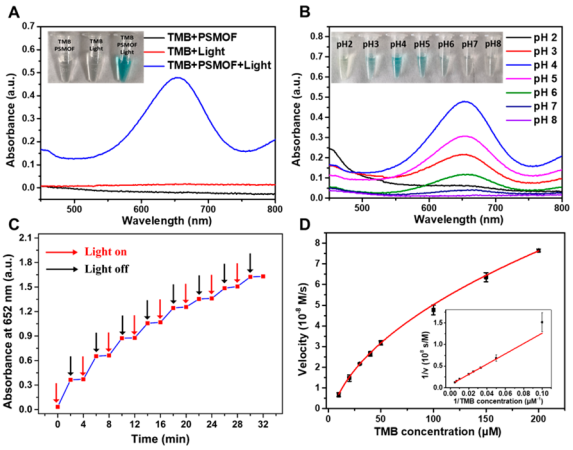

Figure 2. (A) UV−vis absorption spectra of three samples in 0.10 M acetate buffer (pH 4.0) containing the PSMOF + TMB (no light irradiation), TMB under light irradiation, and the PSMOF + TMB (under light irradiation). Inset: corresponding photograph of the three samples. (B) Effects of pH on the oxidase-mimicking activity of the PSMOF. Inset: corresponding photograph of the seven samples. (C) Staircase-like behavior of oxidase-mimicking activity while the light source is turned off and on, indicated by black and reddish arrows, respectively. (D) Steady-state kinetic assay of the PSMOF by varying concentration of TMB. Inset: Lineweaver−Burk plot of photocatalytic activity of the PSMOF with TMB as the substrate.

colored product nor characteristic absorption, which indicated that the light irradiation was critical for the oxidase-like activity of the PSMOF. Furthermore, in absence of the PSMOF, TMB could not be oxidized under the visible-light irradiation either. The above results confirmed that the PSMOF had a visible-light-induced oxidase-mimicking activity. To maximize the oxidase-like activity of the PSMOF, we have optimized the reaction conditions by varying pH values, PSMOF concentrations, and light irradiation time. As shown in Figures 2B and S5, the optimal pH value was 4.0. The oxidase-like activity increased with longer irradiation time and higher PSMOF concentration. Figure S6 showed the irradiation wavelength-dependent oxidase-like activity, which was consistent with the absorption of the PSMOF. The effects of light source on the photocatalysis activity were shown in Figure S7, indicating that a Xe lamp was more suitable for efficiently driving the catalysis compared with a LED lamp. TEM imaging showed the stable structure of the PSMOF after 2 min of catalytic reaction, though the PSMOF was partially degraded under an acidic condition for 2 days (Figure S8). Moreover, to expand the substrate scope of the PSMOF, the catalytic oxidation of OPD and ABTS has also been investigated. As shown in Figure S9, both of them were oxidized by the PSMOF under light irradiation.

In Figure 2C, by successively turning off and on the light irradiation, the oxidase-mimicking activity of the PSMOF exhibited a staircase-like behavior, indicating photocontrollable oxidase-like activity of the PSMOF. In addition, steady-state kinetics was used to characterize the oxidase-like activity of the PSMOF. As shown in Figure 2D and Table S1, typical Michaelis−Menten curves were obtained and kinetic parameters (i.e., v_{max} and K_m) were calculated based on the function: $v = v_{max}[S]/(K_m + [S])$, where v is the initial velocity, $[S]$ is the concentration of substrate, and v_{max} and K_m refer to the maximum reaction velocity and the Michaelis constant, respectively. The PSMOF nanozyme showed a higher v_{max}

DOI: 10.1021/acs.analchem.9b00512
Anal. Chem. 2019, 91, 8170−8175

value for TMB compared with laccase, suggesting that the MOF-based nanozyme efficiently catalyzed the oxidation of oxidase substrates.

Mechanism of the Oxidase-Mimicking Activity of the PSMOF. For the oxidase-mimicking activity of the PSMOF, several possible reactive species could be involved, including hydroxyl radicals ($^{\bullet}OH$), singlet oxygen ($^1O_2$), hydrogen peroxide (H_2O_2), superoxide anion ($O_2^{\bullet-}$), and photogenerated holes (h^+). Selective quenchers were used to probe these reactive species,[53] which would help to elucidate the catalytic mechanism of the PSMOF. Mannitol, tryptophan, catalase (CAT), superoxide dismutase (SOD), and ethanol were selected as the scavengers for eliminating $^{\bullet}OH$, $^1O_2$, H_2O_2, $O_2^{\bullet-}$, and h^+, respectively.

As shown in Figure 3A, the oxidase-like activity of the PSMOF decreased significantly by introducing the scavengers

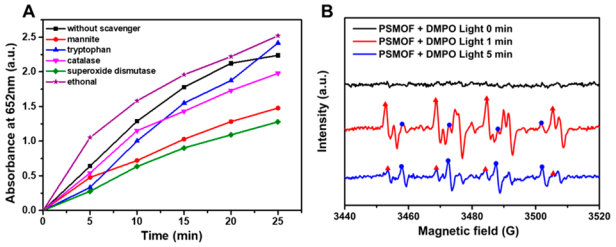

Figure 3. (A) Effect of different scavengers on the catalytic oxidation of TMB by the PSMOF under light irradiation. (B) ESR spectra of the PSMOF and DMPO mixed solution before and after irradiation with Xe lamp (300 W) for 1 and 5 min (red triangle patterns on the top of peaks represent $O_2^{\bullet-}$, and blue circular patterns represent $^{\bullet}OH$).

of mannitol and SOD. However, the scavengers of tryptophan and CAT had little effect on the catalytic reaction. Ethanol even promoted the TMB oxidation, which meant that the quenching of photogenerated holes might inhibit the recombination of electrons and holes, then accelerating the oxidase-like activity.[54] The above test suggested that the formation of $^{\bullet}OH$ and $O_2^{\bullet-}$ during the oxidase-mimicking catalysis.

To further identify the reactive oxygen species (ROS) involved, electron spin resonance (ESR) spectroscopy was employed, which would probe the generation of ROS by using DMPO as a spin trap. In the first minute of irradiation, the vast majority of the ROS product was $O_2^{\bullet-}$ with only a small amount of $^{\bullet}OH$ (Figure 3B, red line). However, after the irradiation time was extended to 5 min, the majority of the ROS product was $^{\bullet}OH$ with only a small amount of $O_2^{\bullet-}$, suggesting the rapid transformation of $O_2^{\bullet-}$ to $^{\bullet}OH$ (Figure 3B, blue line). Combined with the above results, the $O_2^{\bullet-}$ and $^{\bullet}OH$ were the main ROS for the oxidase-mimicking catalysis of the PSMOF.

Colorimetric Detection of Glutathione. Glutathione (GSH) is one of the most abundant antioxidants in organisms. The abnormally intracellular level of GSH is often related to various diseases, including damaged liver,[55] cancer,[56] human immunodeficiency virus (HIV),[57] and Parkinson's disease.[58] As a result of its efficient ROS eliminating ability, the oxidase-mimicking activity of the PSMOF could be inhibited by GSH. On the basis of this interesting phenomenon, we applied the PSMOF as a functional colorimetric probe for GSH detection.

To study the impact of GSH on the oxidase-like activity of the PSMOF, TMB as an oxidase substrate was used for signaling. As depicted in Figure 4A,B, the characteristic UV−vis absorption of TMB_{ox} gradually decreased with increasing the GSH concentration from 0 to 40 μM, indicating the efficient inhibition of GSH toward PSMOF catalysis. In addition, Figure 4C showed a linear relationship between the absorbance at 652 nm and GSH concentration in the range from 0 to 20 μM with R^2 = 0.9842. The detection limit was ~0.68 μM ($S = 3\sigma$), indicating the high sensitivity of the PSMOF probe for the detection of GSH.

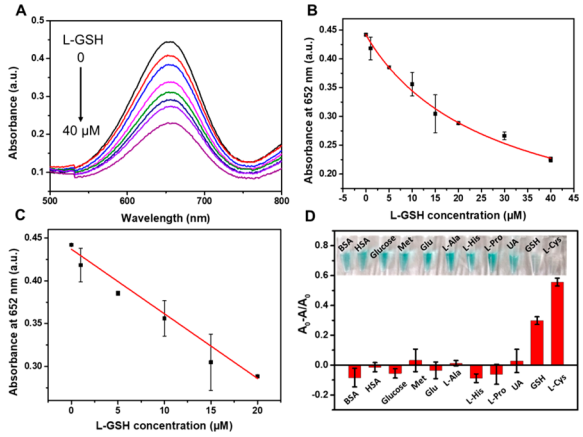

Figure 4. (A) UV−vis absorption spectra of PSMOF-oxidized TMB in the absence and presence of GSH at different concentrations (0−40 μM). (B) The plot of absorbance at 652 nm versus GSH concentration. (C) The linear calibration plotted in the concentration range from 0 to 20 μM. (D) Selectivity of the PSMOF sensor. The concentrations of L-Cys and GSH are 50 μM. The concentrations of BSA and HSA are 10 μM. The UA concentration is 100 μM. The others are 1 mM. Each error bar shows the standard deviation of three independent measurements.

To further evaluate the selectivity of the colorimetric sensor, a variety of common biological interfering species were tested for their effects on GSH detection, including bovine serum albumin (BSA), human serum albumin (HSA), glucose, DL-methionine (Met), glutamic acid (Glu), L-alanine (L-Ala), L-histidine (L-His), L-proline (L-Pro), uric acid (UA), and L-cysteine (L-Cys). As shown in Figure 4D, except L-Cys, all the others had negligible interference on the detection of GSH, probably because of their limited antioxidant capability as well as the excellent anti-interference property of the PSMOF. The observed interference of L-Cys should be from its free sulfhydryl group (−SH), which could inhibit the oxidase-like activity of the PSMOF by scavenging the ROS intermediate in a concentration-dependent manner (Figure S11). Fortunately, the GSH concentration (0.5−10 mM) is much higher than that of L-Cys (30−200 μM) in mammalian cells,[59] indicating that the interference from L-Cys could be neglected. Figure S12 showed that the strong antioxidation activity of ascorbic acid (AA) inhibited the oxidase-mimicking activity of the PSMOF, indicating that the PSMOF did not have selectivity toward strong antioxidants. However, the intracellular AA was depleted over 96% during cell culture, so the presence of AA would not affect the detection of cellular GSH. These results implied that the PSMOF had reasonable selectivity for the detection of GSH.

DOI: 10.1021/acs.analchem.9b00512
Anal. Chem. 2019, 91, 8170−8175

The PSMOF was further employed to evaluate the GSH level in both normal (LO2) and cancer (HeLa) cells. As shown in Figure 5A,B, the characteristic absorbance of TMB_{ox}

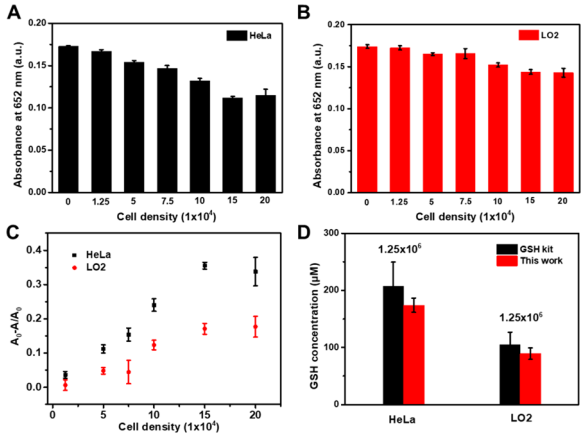

Figure 5. (A,B) Absorbance at 652 nm of TMB after catalytic oxidation with the PSMOF in the absence and presence of HeLa and LO2 cells, respectively. (C) The plot of $(A_0 - A)/A_0$ versus the cell density. A, absorbance at 652 nm in the absence of cells. A_0, absorbance at 652 nm in the presence of cells. (D) Qualitative evaluation of cellular GSH levels with the developed sensor and a GSH kit. The number marked on the histogram is the cell density. Each error bar shows the standard deviation of three independent measurements.

gradually decreased with increasing the cell densities (cells/mL) from 1.25×10^4 to 20×10^4 for both HeLa and LO2 cells, as a result of the efficient inhibition of cellular GSH toward the oxidase-like catalysis. The about 2-fold stronger inhibition effect of HeLa cells than that of LO2 cells could be attributed to the two times higher GSH concentration in tumor cells than that in normal cells (Figure 5C).[60] To further validate the proposed assay for GSH, a commercial GSH kit was employed to evaluate the cellular GSH levels (Figures S13A,B). As shown in Figure 5D, the results of our method matched well with the GSH assay kit, both of which were in consistent with previously reported data.[61] These results demonstrated that the PSMOF nanozyme acted as a reliable functional probe for cellular GSH evaluation.

CONCLUSIONS

In summary, we have developed a light-responsive metal–organic framework with oxidase-like activity. Under visible-light irradiation, the PSMOF catalytically oxidized typical substrates of oxidases such as TMB, OPD, and ABTS by using the dissolved oxygen. We further demonstrated that the oxidase-like activity of the PSMOF could be modulated by switching the "on/off" state of light. By taking advantage of the PSMOF nanozyme, we constructed an effective, sensitive, and selective colorimetric sensor for the detection of GSH in both normal and cancer cells. This study not only provides a smart strategy to modulate nanozymes' activities, but it also broadens the sensing applications of nanozymes. Given the structural and functional diversities of MOFs, we expect that more MOF nanozymes with tunable activities will be developed for future applications.

ASSOCIATED CONTENT

Supporting Information

The Supporting Information is available free of charge on the ACS Publications website at DOI: 10.1021/acs.analchem.9b00512.

Extra figures with associated discussion; tables (PDF)

AUTHOR INFORMATION

Corresponding Author

*E-mail: weihui@nju.edu.cn; Tel: +86-25-83593272; Fax: +86-25-83594648.

ORCID

Xiaoyu Wang: 0000-0002-8641-2430

Hui Wei: 0000-0003-0870-7142

Author Contributions

The manuscript was written through contributions of all authors. All authors have given approval to the final version of the manuscript.

Notes

The authors declare no competing financial interest.

ACKNOWLEDGMENTS

This work was supported by the National Natural Science Foundation of China (21722503, 21874067, and 91859112), 973 Program (2015CB659400), PAPD Program, Shuangchuang Program of Jiangsu Province, Open Funds of the State Key Laboratory of Analytical Chemistry for Life Science (SKLACLS1704), Open Funds of the State Key Laboratory of Coordination Chemistry (SKLCC1819), Open Funds of the Key Laboratory of Analytical Chemistry for Biology and Medicine (Ministry of Education) (ACBM2019001), and Fundamental Research Funds for the Central Universities (021314380145). The authors thank Prof. Kang Wang and Zhongqiu Li for help with the measurements of wavelength-dependent oxidase-mimicking activity.

REFERENCES

(1) Gao, L.; Zhuang, J.; Nie, L.; Zhang, J.; Zhang, Y.; Gu, N.; Wang, T.; Feng, J.; Yang, D.; Perrett, S.; Yan, X. *Nat. Nanotechnol.* **2007**, *2*, 577–583.

(2) Wei, H.; Wang, E. *Anal. Chem.* **2008**, *80*, 2250–2254.

(3) Manea, F.; Houillon, F. B.; Pasquato, L.; Scrimin, P. *Angew. Chem., Int. Ed.* **2004**, *43*, 6165–6169.

(4) Wei, H.; Wang, E. *Chem. Soc. Rev.* **2013**, *42*, 6060–6093.

(5) Lin, Y.; Ren, J.; Qu, X. *Acc. Chem. Res.* **2014**, *47*, 1097–1105.

(6) Wang, X.; Hu, Y.; Wei, H. *Inorg. Chem. Front.* **2016**, *3*, 41–60.

(7) Zhang, Z.; Zhang, X.; Liu, B.; Liu, J. *J. Am. Chem. Soc.* **2017**, *139*, 5412–5419.

(8) Tonga, G. Y.; Jeong, Y.; Duncan, B.; Mizuhara, T.; Mout, R.; Das, R.; Kim, S. T.; Yeh, Y.-C.; Yan, B.; Hou, S.; Rotello, V. M. *Nat. Chem.* **2015**, *7*, 597–603.

(9) Gao, Z.; Ye, H.; Tang, D.; Tao, J.; Habibi, S.; Minerick, A.; Tang, D.; Xia, X. *Nano Lett.* **2017**, *17*, 5572–5579.

(10) Kim, M. S.; Kweon, S. H.; Cho, S.; An, S. S. A.; Kim, M. I.; Doh, J.; Lee, J. *ACS Appl. Mater. Interfaces* **2017**, *9*, 35133–35140.

(11) Wang, Q.; Zhang, X.; Huang, L.; Zhang, Z.; Dong, S. *Angew. Chem., Int. Ed.* **2017**, *56*, 16082–16085.

(12) Tarnuzzer, R. W.; Colon, J.; Patil, S.; Seal, S. *Nano Lett.* **2005**, *5*, 2573–2577.

(13) Chen, W.-H.; Vazquez-Gonzalez, M.; Zoabi, A.; Abu-Reziq, R.; Willner, I. *Nat. Catal.* **2018**, *1*, 689–695.

(14) Walther, R.; Winther, A. K.; Fruergaard, A. S.; van den Akker, W.; Sorensen, L.; Nielsen, S. M.; Jarlstad Olesen, M. T.; Dai, Y.;

DOI: 10.1021/acs.analchem.9b00512
Anal. Chem. 2019, 91, 8170–8175

Jeppesen, H. S.; Lamagni, P.; Savateev, A.; Pedersen, S.-E. L.; Frich, C. K.; Vigier-Carriere, C.; Lock, N.; Singh, M.; Bansal, V.; Meyer, R. L.; Zelikin, A. N. *Angew. Chem., Int. Ed.* **2019**, *58*, 278−282.
(15) Xu, Z.; Qiu, Z.; Liu, Q.; Huang, Y.; Li, D.; Shen, X.; Fan, K.; Xi, J.; Gu, Y.; Tang, Y.; Jiang, J.; Xu, J.; He, J.; Gao, X.; Liu, Y.; Koo, H.; Yan, X.; Gao, L. *Nat. Commun.* **2018**, *9*, 3713.
(16) Shen, X.; Liu, W.; Gao, X.; Lu, Z.; Wu, X.; Gao, X. *J. Am. Chem. Soc.* **2015**, *137*, 15882−15891.
(17) Asati, A.; Santra, S.; Kaittanis, C.; Nath, S.; Perez, J. M. *Angew. Chem., Int. Ed.* **2009**, *48*, 2308−2312.
(18) Zhou, Y.; Liu, B.; Yang, R.; Liu, J. *Bioconjugate Chem.* **2017**, *28*, 2903−2909.
(19) Wu, J.; Wang, X.; Wang, Q.; Lou, Z.; Li, S.; Zhu, Y.; Qin, L.; Wei, H. *Chem. Soc. Rev.* **2019**, *48*, 1004−1076.
(20) Ishida, T.; Kinoshita, N.; Okatsu, H.; Akita, T.; Takei, T.; Haruta, M. *Angew. Chem., Int. Ed.* **2008**, *47*, 9265−9268.
(21) Peng, F. F.; Zhang, Y.; Gu, N. *Chin. Chem. Lett.* **2008**, *19*, 730−733.
(22) Singh, N.; Savanur, M. A.; Srivastava, S.; D'Silva, P.; Mugesh, G. *Angew. Chem., Int. Ed.* **2017**, *56*, 14267−14271.
(23) Liu, S.; Lu, F.; Xing, R.; Zhu, J.-J. *Chem. - Eur. J.* **2011**, *17*, 620−625.
(24) Kluenker, M.; Nawaz Tahir, M.; Ragg, R.; Korschelt, K.; Simon, P.; Gorelik, T. E.; Barton, B.; Shylin, S. I.; Panthoefer, M.; Herzberger, J.; Frey, H.; Ksenofontov, V.; Moeller, A.; Kolb, U.; Grin, J.; Tremel, W. *Chem. Mater.* **2017**, *29*, 1134−1146.
(25) Korsvik, C.; Patil, S.; Seal, S.; Self, W. T. *Chem. Commun.* **2007**, 1056−1058.
(26) Wang, X.; Cao, W.; Qin, L.; Lin, T.; Chen, W.; Lin, S.; Yao, J.; Zhao, X.; Zhou, M.; Hang, C.; Wei, H. *Theranostics* **2017**, *7*, 2277−2286.
(27) Islamoglu, T.; Atilgan, A.; Moon, S.-Y.; Peterson, G. W.; DeCoste, J. B.; Hall, M.; Hupp, J. T.; Farha, O. K. *Chem. Mater.* **2017**, *29*, 2672−2675.
(28) Celardo, I.; De Nicola, M.; Mandoli, C.; Pedersen, J. Z.; Traversa, E.; Ghibelli, L. *ACS Nano* **2011**, *5*, 4537−4549.
(29) Wang, Q.; Zhang, X.; Huang, L.; Zhang, Z.; Dong, S. *ACS Appl. Mater. Interfaces* **2017**, *9*, 7465−7471.
(30) Sun, X.; Guo, S.; Chung, C.-S.; Zhu, W.; Sun, S. *Adv. Mater.* **2013**, *25*, 132−136.
(31) Ouyang, H.; Tu, X.; Fu, Z.; Wang, W.; Fu, S.; Zhu, C.; Du, D.; Lin, Y. *Biosens. Bioelectron.* **2018**, *106*, 43−49.
(32) Asati, A.; Kaittanis, C.; Santra, S.; Perez, J. M. *Anal. Chem.* **2011**, *83*, 2547−2553.
(33) Xu, C.; Liu, Z.; Wu, L.; Ren, J.; Qu, X. *Adv. Funct. Mater.* **2014**, *24*, 1624−1630.
(34) Zhan, L.; Li, C. M.; Wu, W. B.; Huang, C. Z. *Chem. Commun.* **2014**, *50*, 11526−11528.
(35) Neri, S.; Garcia Martin, S.; Pezzato, C.; Prins, L. J. *J. Am. Chem. Soc.* **2017**, *139*, 1794−1797.
(36) Zhang, J.; Lu, X.; Tang, D.; Wu, S.; Hou, X.; Liu, J.; Wu, P. *ACS Appl. Mater. Interfaces* **2018**, *10*, 40808−40814.
(37) Zhao, Y.; Lei, B.; Wang, M.; Wu, S.; Qi, W.; Su, R.; He, Z. *J. Mater. Chem. B* **2018**, *6*, 2444−2449.
(38) Chong, Y.; Ge, C.; Fang, G.; Tian, X.; Ma, X.; Wen, T.; Wamer, W. G.; Chen, C.; Chai, Z.; Yin, J.-J. *ACS Nano* **2016**, *10*, 8690−8699.
(39) Zhang, J.; Wu, S.; Lu, X.; Wu, P.; Liu, J. *Nano Lett.* **2019**, *19*, 3214−3220.
(40) Wang, C.; Shi, Y.; Dan, Y.-Y.; Nie, X.-G.; Li, J.; Xia, X.-H. *Chem. - Eur. J.* **2017**, *23*, 6717−6723.
(41) Wang, G.-L.; Jin, L.-Y.; Dong, Y.-M.; Wu, X.-M.; Li, Z.-J. *Biosens. Bioelectron.* **2015**, *64*, 523−529.
(42) Jin, L.-Y.; Dong, Y.-M.; Wu, X.-M.; Cao, G.-X.; Wang, G.-L. *Anal. Chem.* **2015**, *87*, 10429−10436.
(43) Wang, G.-L.; Xu, X.-F.; Qiu, L.; Dong, Y.-M.; Li, Z.-J.; Zhang, C. *ACS Appl. Mater. Interfaces* **2014**, *6*, 6434−6442.
(44) Cui, Y.; Yue, Y.; Qian, G.; Chen, B. *Chem. Rev.* **2012**, *112*, 1126−1162.
(45) Lustig, W. P.; Mukherjee, S.; Rudd, N. D.; Desai, A. V.; Li, J.; Ghosh, S. K. *Chem. Soc. Rev.* **2017**, *46*, 3242−3285.
(46) Zhang, T.; Lin, W. *Chem. Soc. Rev.* **2014**, *43*, 5982−5993.
(47) Hu, Y.; Cheng, H.; Zhao, X.; Wu, J.; Muhammad, F.; Lin, S.; He, J.; Zhou, L.; Zhang, C.; Deng, Y.; Wang, P.; Zhou, Z.; Nie, S.; Wei, H. *ACS Nano* **2017**, *11*, 5558−5566.
(48) Cheng, H.; Liu, Y.; Hu, Y.; Ding, Y.; Lin, S.; Cao, W.; Wang, Q.; Wu, J.; Muhammad, F.; Zhao, X.; Zhao, D.; Li, Z.; Xing, H.; Wei, H. *Anal. Chem.* **2017**, *89*, 11552−11559.
(49) Cheng, H.; Zhang, L.; He, J.; Guo, W.; Zhou, Z.; Zhang, X.; Nie, S.; Wei, H. *Anal. Chem.* **2016**, *88*, 5489−5497.
(50) Qin, L.; Wang, X.; Liu, Y.; Wei, H. *Anal. Chem.* **2018**, *90*, 9983−9989.
(51) Wang, C.; Lin, W. *J. Am. Chem. Soc.* **2011**, *133*, 4232−4235.
(52) Kober, E. M.; Meyer, T. J. *Inorg. Chem.* **1982**, *21*, 3967−3977.
(53) Wang, H.; Jiang, S.; Chen, S.; Li, D.; Zhang, X.; Shao, W.; Sun, X.; Xie, J.; Zhao, Z.; Zhang, Q.; Tian, Y.; Xie, Y. *Adv. Mater.* **2016**, *28*, 6940−6945.
(54) Waiskopf, N.; Ben-Shahar, Y.; Galchenko, M.; Carmel, I.; Moshitzky, G.; Soreq, H.; Banin, U. *Nano Lett.* **2016**, *16*, 4266−4273.
(55) Lu, S. C. *Mol. Aspects Med.* **2009**, *30*, 42−59.
(56) Townsend, D. M.; Tew, K. D.; Tapiero, H. *Biomed. Pharmacother.* **2003**, *57*, 145−155.
(57) Herzenberg, L. A.; DeRosa, S. C.; Dubs, J. G.; Roederer, M.; Anderson, M. T.; Ela, S. W.; Deresinski, S. C.; Herzenberg, L. A. *Proc. Natl. Acad. Sci. U. S. A.* **1997**, *94*, 1967−1972.
(58) Smeyne, M.; Smeyne, R. J. *Free Radical Biol. Med.* **2013**, *62*, 13−25.
(59) Liu, J.; Sun, Y.-Q.; Huo, Y.; Zhang, H.; Wang, L.; Zhang, P.; Song, D.; Shi, Y.; Guo, W. *J. Am. Chem. Soc.* **2014**, *136*, 574−577.
(60) Perry, R. R.; Mazetta, J.; Levin, M.; Barranco, S. C. *Cancer* **1993**, *72*, 783−787.
(61) Wei, C.; Liu, X.; Gao, Y.; Wu, Y.; Guo, X.; Ying, Y.; Wen, Y.; Yang, H. *Anal. Chem.* **2018**, *90*, 11333−11339.

DOI: 10.1021/acs.analchem.9b00512
Anal. Chem. 2019, 91, 8170−8175